

## Supporting Information

### **Fast and Scalable Wet-spinning of Highly Conductive PEDOT:PSS Fibers Enables Versatile Applications**

*Jizhen Zhang, Shayan Seyedin, Si Qin,\* Peter A. Lynch, Zhiyu Wang, Wenrong Yang, Xungai Wang, Joselito M. Razal\**

J. Zhang, Dr. S. Seyedin, Dr. S. Qin, Dr. P. A. Lynch, Z. Wang, Prof. X. Wang, A/Prof. J. M. Razal

Institute for Frontier Materials, Deakin University, Geelong, Victoria 3216, Australia

E-mail: si.qin@deakin.edu.au, joselito.razal@deakin.edu.au,

Dr. W. Yang

School of Life and Environmental Sciences, Deakin University, Geelong, Victoria 3216, Australia

**Video S1.** PEDOT:PSS fiber ( $P_1$  fiber) in boiling water.

**Video S2.** Comparison of the wet strength of  $P_{IPA}$  and  $P_1$  fibers.

## 1. Supporting experimental

### 1.1. Calculation of electrical conductivity

The electrical conductivity of the PEDOT:PSS fiber was measured using a source meter unit (Keysight B2901A) by the aid of a custom-built four-point probe set-up. The four-point probe electrical conductivity ( $\sigma$ , S cm<sup>-1</sup>) of the fiber samples was calculated using Equation (S1):

$$\sigma = \frac{4 \cdot l}{\pi \cdot d^2 \cdot R} \quad (\text{S1})$$

where  $R$  is the resistance of the fiber ( $\Omega$ ) calculated from the  $I$  vs.  $V$  curve,  $l$  is the length of the tested fiber sample between the middle two electrodes, measured as 0.253 cm for our custom-built set-up, and  $d$  is the nominal diameter of the fiber (cm).

The cyclic voltammetry (CV) curves of the fibers were obtained using a two-electrode configuration. Two PEDOT:PSS fibers were placed in parallel on a PET foil and coated with PVA/H<sub>3</sub>PO<sub>4</sub> electrolyte. The gel electrolyte was prepared by dissolving 10 g of PVA and 10 g of H<sub>3</sub>PO<sub>4</sub> in 100 mL of deionized water. Then device were dried in air for 12 h before testing. The reserved electrode heads were connected to metal wires by silver paste for the electrochemical tests using an electrochemical workstation (BioLogic SP-300). The CV curves were recorded at a potential window of 0 to 1.0 V at scan rates ranging from 5 to 2000 mV s<sup>-1</sup>. The cyclic stability test was performed at 500 mV s<sup>-1</sup> for 10,000 cycles.

The capacitance of the two-electrode device ( $C_D$ ) was calculated from the CV and GCD curves according to the Equations (S2):

$$C_D = \frac{\int IdU}{2v\Delta U} \quad (\text{S2})$$

where  $I$  is the discharge current,  $v$  is the potential scan rate (V s<sup>-1</sup>),  $\Delta U$  is the potential window (V), and  $dU/dt$  is the slope of the discharge curve in GCD.

The gravimetric capacitance ( $C_M$ , F g<sup>-1</sup>) and volumetric capacitance ( $C_V$ , F cm<sup>-3</sup>) of the electrodes were calculated based on the device capacitance ( $C_D$ ) using Equations (S3) and (S4), respectively.

$$C_M = \frac{2C_D}{m} \quad (\text{S3})$$

$$C_V = \frac{2C_D}{v} \quad (\text{S4})$$

where  $m$  and  $v$  are the mass and volume of one single electrode, respectively.

The capacitance retention ( $C_r$ ) was calculated from the specific capacitance of electrode ( $C_i$ ) in the cycle  $i$  and the specific capacitance in the first cycle ( $C_1$ ) using the Equation (S5).

$$C_r = \frac{C_i}{C_1} \times 100\% \quad (\text{S5})$$

For capacitive sensing, a capacitance ( $C_f$ ) is formed between finger and electrode. The processor (Arduino uno R3) was used to recognize the change in capacitance. The humidity sensing experiment was performed using a custom-built humidity control system (Figure S10a). The resistance of the fiber was recorded using a digital multimeter (Keysight 34461A) using a four-point probe set-up. All data were collected at room temperature.

### 1.2. Calculation of shear rate

The shear rate ( $\gamma$ , s<sup>-1</sup>) for a Newtonian fluid was calculated using the Equation (S6):

$$\gamma = \frac{4Q}{\pi \cdot R^3} \quad (\text{S6})$$

where  $Q$  and  $R$  are the flow rate (m<sup>3</sup> s<sup>-1</sup>) and the radius of the nozzle (m), respectively.

### 1.3. Calculation of the crystalline size

The size of the crystalline domains in PEDOT:PSS fiber was calculated from the broadening of peaks in diffraction patterns, using the Scherrer formula (Equation S7):

$$\tau = \frac{K\lambda}{\beta \cos\theta} \quad (\text{S7})$$

where  $\tau$  is the average size of the crystalline domains;  $K$  is a dimensionless shape factor (a typical value of 0.94 in our calculation);  $\lambda$  is the X-ray wavelength;  $\beta$  is the line broadening at half the maximum intensity (FWHM) after subtracting the instrumental line broadening in radians;  $\theta$  is the Bragg angle in degree.

#### 1.4. Calculation of Herman's orientation function

Herman's orientation factor ( $f$ ) was calculated to describe the degree of orientation of the PEDOT:PSS chain axis relative to the fiber axis using Equation (S8):

$$f = \frac{3(\langle \cos^2 \vartheta \rangle) - 1}{2} \quad (\text{S8})$$

where the mean-square cosine is calculated from the scattered intensity  $I(\vartheta)$  by integrating over the azimuthal angle  $\vartheta$ , Equation (S9):

$$\langle \cos^2 \vartheta \rangle = \frac{\int_0^{\pi/2} I(\vartheta) \sin \vartheta \cos^2 \vartheta d\vartheta}{\int_0^{\pi/2} I(\vartheta) \sin \vartheta d\vartheta} \quad (\text{S9})$$

where  $\vartheta$  is the angle between fiber axis and the polymer-chain axis.  $f = 1$  when all polymer chains are aligned with the fiber axis and  $f = 0$  for a randomly oriented polymer chains.

## 2. Supporting results and discussions

**Table S1.** Summary of PEDOT:PSS treatment methods reported in the literature.

Method	Treatment compound	Mechanism	Pristine conductivity [S cm <sup>-1</sup> ]	Enhanced conductivity [S cm <sup>-1</sup> ]	Ref.
Addition into formulation	<sup>a)</sup> DMSO, <sup>b)</sup> DMF	Reducing the effective energy barrier for hopping via secondary doping	0.2-1	600-767	1-3
	<sup>c)</sup> EG	Blocking the ionic interactions between PEDOT and PSS, and improving alignment of PEDOT chains	--	767	3, 4
	<sup>d)</sup> PEG	Blocking the ionic interaction between PEDOT and PSS, and improving connections among PEDOT chains	0.3	805	5
Post treatment	Methylammonium iodide in DMF	Segregation of PSS chains and PEDOT chains via the synergistic effects of both organic salts and organic solvents on the microstructure	0.2	1660	6
	<sup>e)</sup> HFA	Conformational changes in the conductive PEDOT chains and phase segregation of PSS chains from PEDOT:PSS	0.3	1164-1325	7
	Methanesulfonic acid	Proton transfer from the mild or weak organic acids to PSS in PEDOT:PSS	0.3	3300	8
	H <sub>2</sub> SO <sub>4</sub>	Reducing the amount of PSS or partial replacement of PSS by SO <sub>4</sub> <sup>2-</sup> , and structural rearrangement in PEDOT:PSS films,	0.3-1	~2400-4380	9, 10
	HNO <sub>3</sub>	Selective removal of PSS domains, and crystallization of PEDOT:PSS	~1	4100	11
Addition + post treatment	DMSO + EG	Same as EG	1	1418	12
	PEG + PEG	Same as PEG	1	1100	5

<sup>a)</sup>Dimethyl sulfoxide, <sup>b)</sup>Dimethylformamide, <sup>c)</sup>Ethylene glycol, <sup>d)</sup>Poly(ethylene glycol),

<sup>e)</sup>Hexafluoroacetone

**Table S2.** Comparison of mechanical and electrical properties of PEDOT:PSS fibers produced in this work with previous reports.

Spinning formulation	Coagulation bath	Post-treatment	Young's modulus [GPa]	Ultimate stress [MPa]	Strain at break [%]	Conductivity [ $S\ cm^{-1}$ ]	Ref.
PEDOT:PSS	H <sub>2</sub> SO <sub>4</sub> (98 wt. %) for 10 mins	--	5.2 ± 0.5	434.8 ± 21.3	25.4 ± 0.6	2640 ± 200	This work (P1 fiber)
PEDOT:PSS with EG	H <sub>2</sub> SO <sub>4</sub> (98 wt. %) for 10 mins	--	3.9 ± 0.3	425.2 ± 11.3	35.9 ± 1.5	3828 ± 400	This work (P4 fiber)
PEDOT:PSS	Acetone	--	1.1	17.2	4.3	< 1	13
PEDOT:PSS	Acetone	Dipping in EG	4.0	130	7.7	467	14
PEDOT:PSS with PEG	Isopropanol	Dipping in EG	2.5	97	13.5	264	15
PEDOT:PSS with SWCNT	Isopropanol	Dipping in EG	5.2	200	12	450	16
PEDOT:PSS	Ethanol and water with CaCl <sub>2</sub>	Dipping in EG	--	80	17	38	17
PEDOT:PSS with EG	Isopropanol	Hot drawing and dipping in EG	8.3	409	21.2	2804	18
PEDOT:PSS with EG	Acetone/ Isopropanol	Hot drawing and dipping in EG	8.3	--	--	3131	19

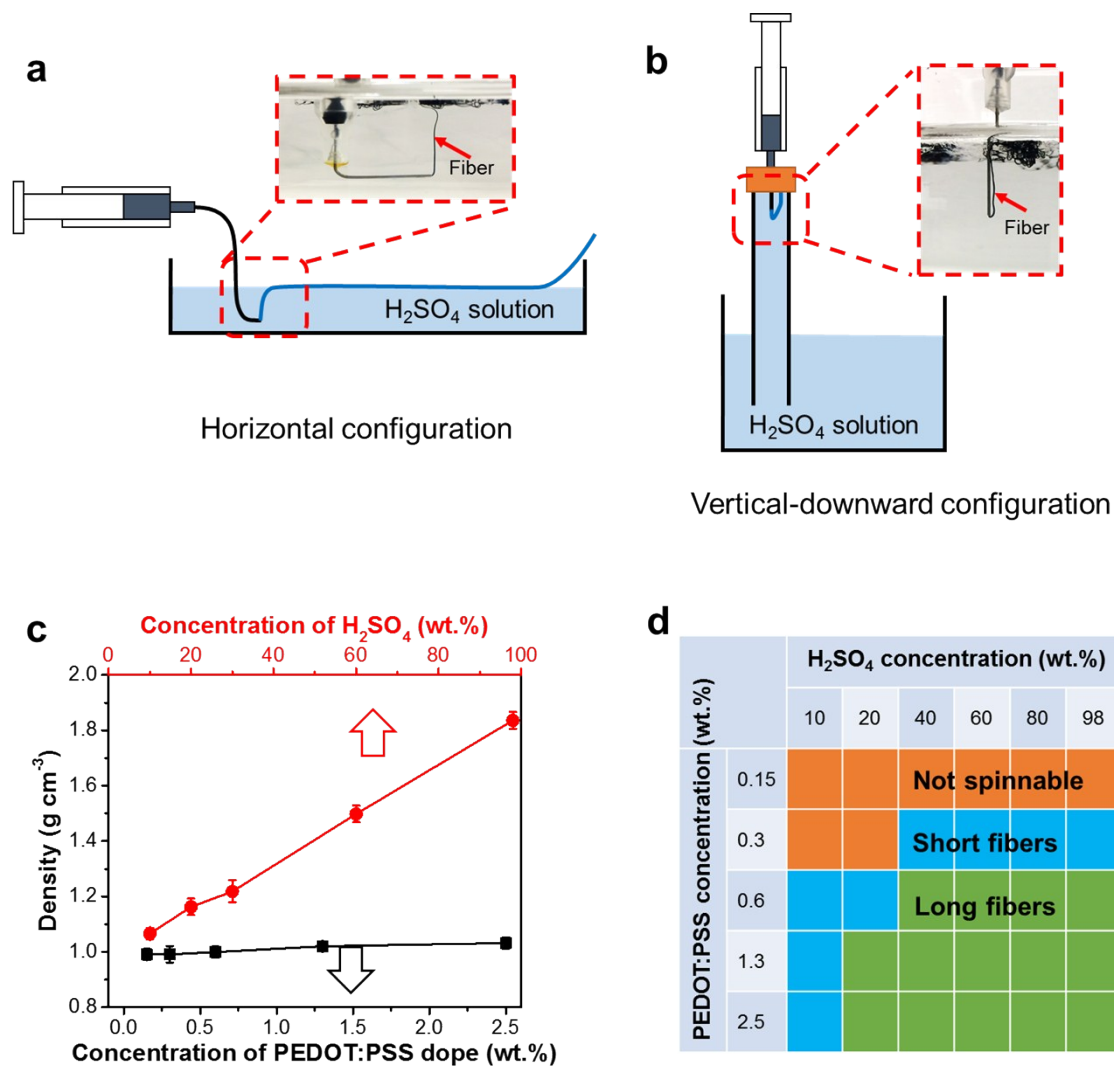


**Fig. S1.** a) The horizontal and b) vertical-downward coagulation configurations used for spinning PEDOT:PSS fiber in H<sub>2</sub>SO<sub>4</sub> solution. c) Densities of H<sub>2</sub>SO<sub>4</sub> solutions and PEDOT:PSS formulations at different concentrations measured at room temperature ~25 °C. d) The spinnability of various PEDOT:PSS dispersion concentrations at different H<sub>2</sub>SO<sub>4</sub> concentrations.

Due to the difference in density, the extruded PEDOT:PSS fiber tends to flow upward. We calculated the buoyancy force ( $F_b$ , N) based on the assumption that there was no change in fiber diameter ( $D \sim 156 \mu\text{m}$ ) and fiber density ( $d \sim 1.0324 \text{ g cm}^{-3}$ ) during fiber spinning. For the coagulation bath with 98 wt. % H<sub>2</sub>SO<sub>4</sub> with 20 cm depth ( $l$ , m), the buoyancy force and acceleration ( $a$ , m s<sup>-2</sup>) were calculated using Equations (S10) and (S11), respectively:

$$F_b = \rho V g = \frac{\rho \pi D^2 l g}{4} \quad (\text{S10})$$

$$a = \frac{F_b - dVg}{dV} = \frac{(\rho - d)g}{d} \quad (\text{S11})$$

In the above equations,  $\rho$ ,  $V$ , and  $g$  represent density of  $\text{H}_2\text{SO}_4$  solution ( $1.8361 \text{ g cm}^{-3}$ ), volume of the fiber and the standard acceleration due to gravity ( $9.8 \text{ m s}^{-2}$ ), respectively.

The spinnability of the formulation improved with increasing PEDOT:PSS and  $\text{H}_2\text{SO}_4$  concentrations (Figure S1d). The 0.15 wt. % PEDOT:PSS dispersion was not spinnable even in 98 wt. %  $\text{H}_2\text{SO}_4$  while only <10 cm fibers could be obtained at 0.30 wt. % PEDOT:PSS. Increasing the concentration of PEDOT:PSS resulted in higher viscosity and better spinnability (Figure S3). In order to spin fibers longer than 10 m, concentrations of PEDOT:PSS and  $\text{H}_2\text{SO}_4$  must be >0.60 wt. % and >20 wt. %, respectively.

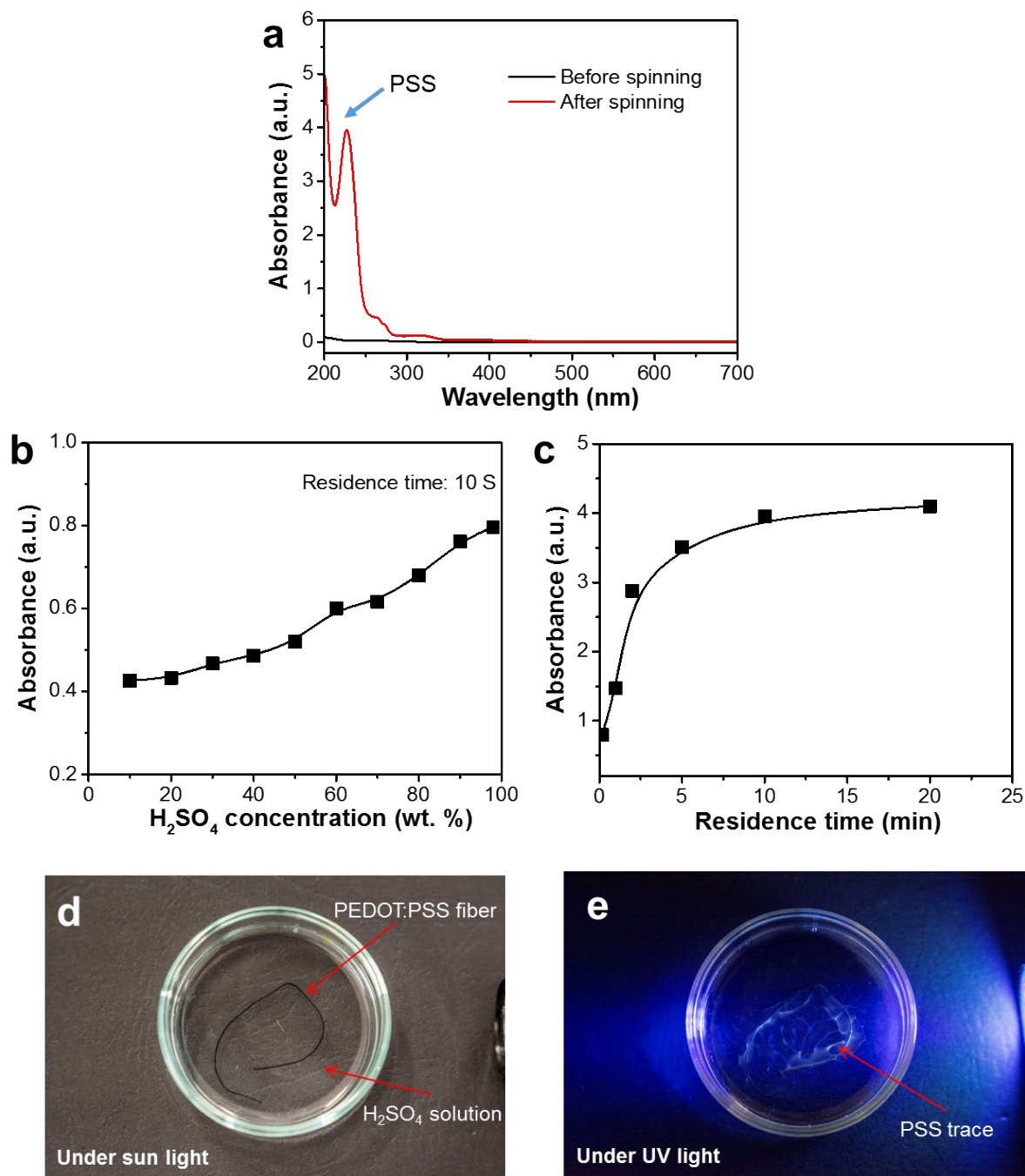


**Fig. S2.** (a) UV-Vis absorption spectra of  $H_2SO_4$  solutions before and after wet-spinning. (b) The absorbance at 226 nm of different concentration of  $H_2SO_4$  bath after spinning PEDOT:PSS. (c) The absorbance at 226 nm of  $H_2SO_4$  bath versus residence time of PEDOT:PSS fiber in the bath. Photographs of PEDOT:PSS fiber immersed in  $H_2SO_4$  solution under (d) ambient light and (e) UV light.

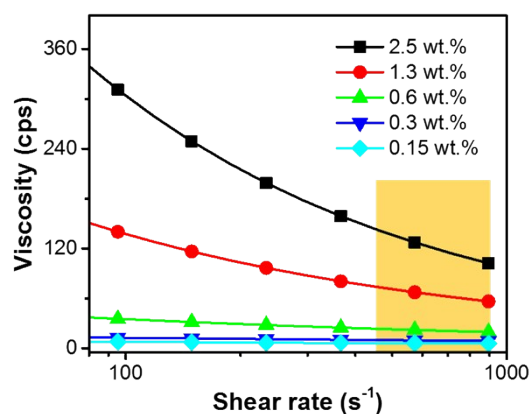


**Fig. S3.** The viscosity of the PEDOT:PSS formulations at various concentrations as a function of shear rate.

The PEDOT:PSS solution shows a typical characteristic of Newtonian fluid (Figure S3). We used Equation (S6) to estimate the shear rate during spinning. In our experiment, a 27 gauge needle (inner diameter of 210  $\mu\text{m}$ ) with flow rates of 1.5 to 3  $\text{mL h}^{-1}$  resulted in shear rates ranging from 458.6 to 916.8  $\text{s}^{-1}$ . Figure S3 shows the rheological properties of the PEDOT:PSS dispersions at different concentrations and the result suggested that a PEDOT:PSS dispersion with a viscosity of at least  $\sim 20$  cP was necessary to achieve continuous fibers. The viscosity of PEDOT:PSS formulation at shear rate of 717  $\text{s}^{-1}$  increased with concentration and experiment results suggested that 1.3 wt. % and 2.5 wt. % of PEDOT:PSS dispersions possessed good spinnability.

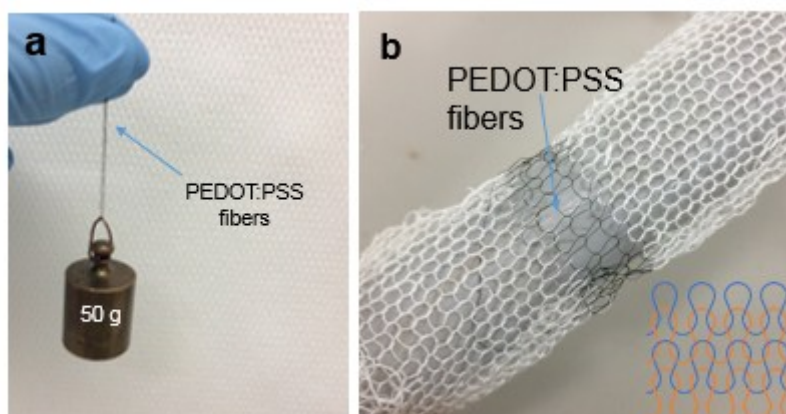


**Fig. S4.** (a) Photo of seven P1 fibers lifting a 50 g weight. (b) Photograph of free-standing textile prototype with P1 fiber made using a conventional knitting machine.

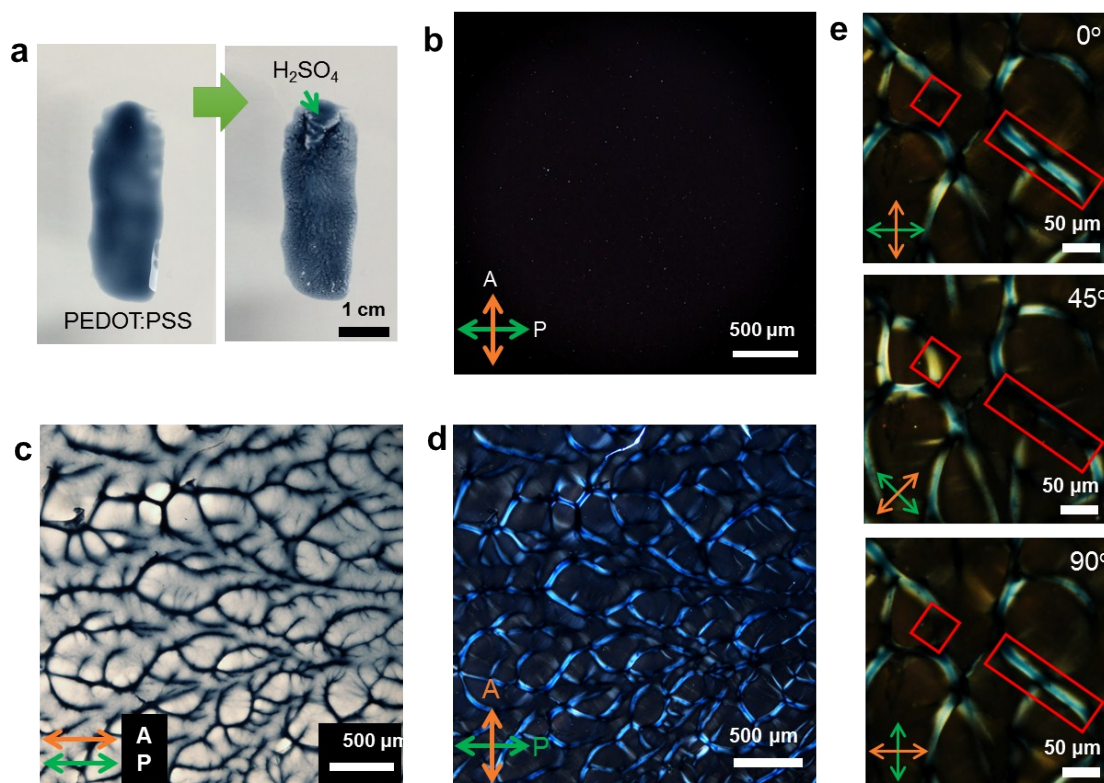


**Fig. S5.** (a) Photographs of PEDOT:PSS suspension (2.5 wt. %) on glass slides. (Left) before and (right) after dropping  $\text{H}_2\text{SO}_4$  solution on one side of the wet film. (b) The polarizing optical microscope (POM) image of pristine PEDOT:PSS solution. The POM images of self-assembled dendritic structure of PEDOT:PSS with polarizer and analyzer (c) in parallel-polarized and (d) cross-polarized positions, respectively. Arrows stands for the transmission axis of the polarizer (P) and analyzer (A), respectively. (e) POM images of the same position with the polarizer and analyzer rotated to  $0^\circ$ ,  $45^\circ$  and  $90^\circ$ .

We observed the changes in POM images upon rotating the polarizer and analyzer from  $0^\circ$  to  $90^\circ$ . As shown in Figure S5e, the bright field and dark field marked with red rectangles turn into dark and bright upon rotation by  $45^\circ$ , respectively. These spots returned to their original brightness when rotated to  $90^\circ$  suggesting alignment of PEDOT:PSS chains upon exposure to  $\text{H}_2\text{SO}_4$  treatment.

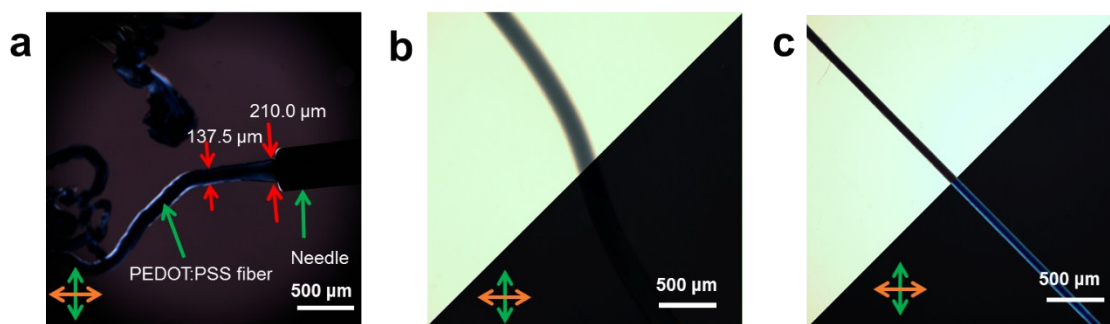


**Fig. S6.** (a) POM image of the initial fiber formation upon extrusion of PEDOT:PSS solution into a  $\text{H}_2\text{SO}_4$  bath. PEDOT:PSS fibers prepared in (b) IPA and (c)  $\text{H}_2\text{SO}_4$  baths observed under bright field (top) and polarized (bottom) configurations.

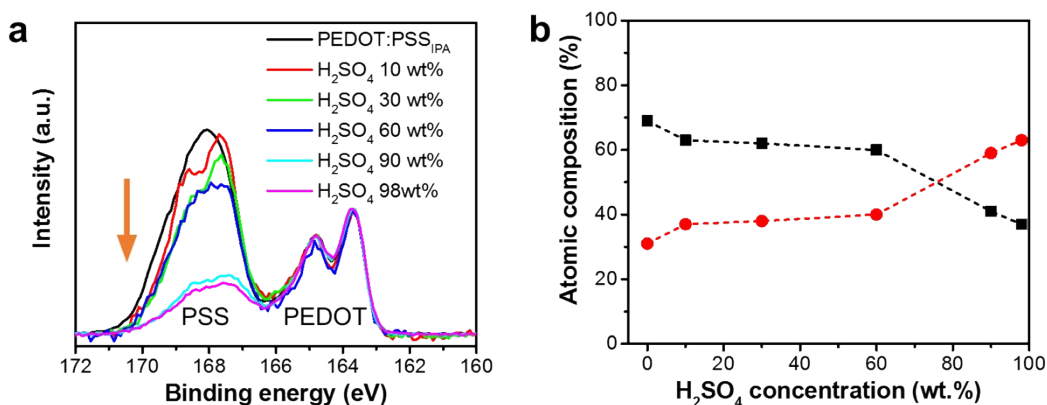


**Fig. S7.** (a) Comparison of X-ray photoelectron spectroscopy (XPS) spectra of the S(2*p*) region for P<sub>IPA</sub> fiber and PEDOT:PSS fibers prepared from different H<sub>2</sub>SO<sub>4</sub> coagulation bath concentrations. (b) The atomic composition of S in PEDOT:PSS fiber as function of H<sub>2</sub>SO<sub>4</sub> coagulation bath concentration. Filled black squares and filled red circles represent S compositions from PSS and PEDOT, respectively.

The S(2*p*) region in the XPS spectra show the different binding energies for sulfur in PEDOT (164.2 eV) and PSS (168.8 eV). The XPS S(2*p*) spectra of PEDOT-PSS fibers give the surface sulfonate/thiophene ratio presumed to be the surface PSS/PEDOT ratio. A high H<sub>2</sub>SO<sub>4</sub> coagulation bath concentration resulted in the decrease in the atomic S composition attributed to PSS illustrating the efficiency of PSS removal with increasing H<sub>2</sub>SO<sub>4</sub> concentration.

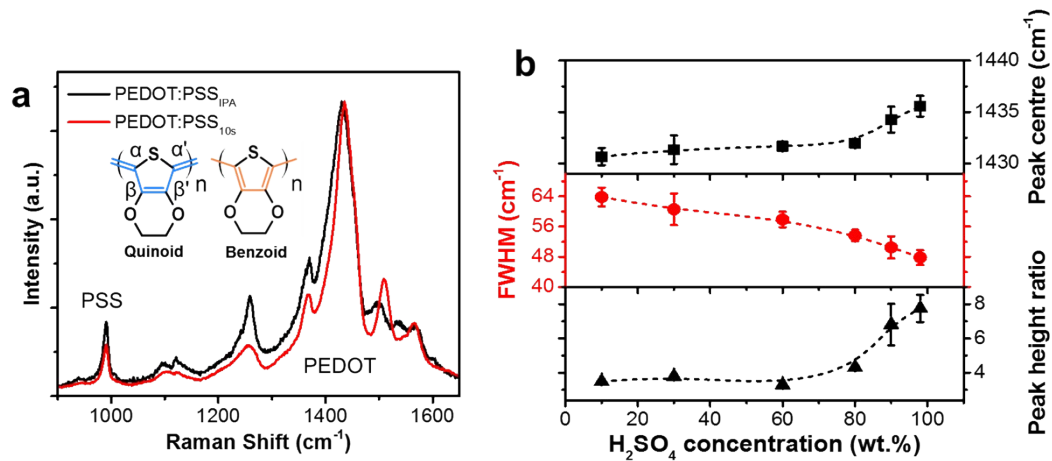


**Fig. S8.** (a) Comparison of the Raman spectra of P<sub>IPA</sub> and P<sub>10s</sub> fibers. P<sub>10s</sub> fiber is a PEDOT:PSS fiber prepared using 98 wt. % H<sub>2</sub>SO<sub>4</sub> coagulation bath and a residence time of 10 seconds. (b) Raman peak analysis of the P<sub>10s</sub> fiber spun using different H<sub>2</sub>SO<sub>4</sub> coagulation bath concentration. (top) Raman peak position, (middle) FWHM for PEDOT and (bottom) peak height ratio relative to the peak at 990 cm<sup>-1</sup> attributed to PSS.

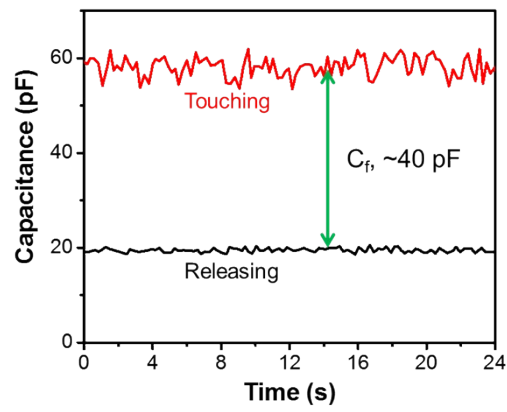


**Fig. S9.** Representative data that illustrate change in capacitance change of  $\sim 40$  pF upon touching of the fiber electrode in the textile capacitive touch sensor prototype.

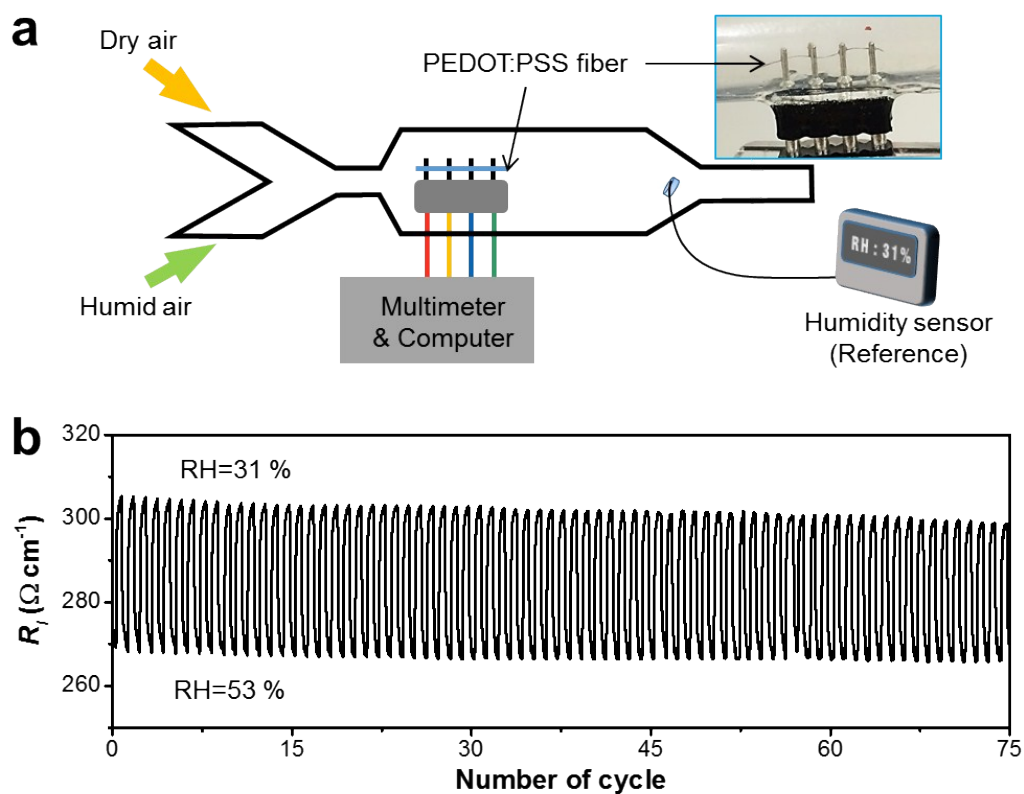


**Fig. S10.** (a) Schematic illustration of the set-up used in measuring the change in resistance of PEDOT:PSS fibers when exposed to various humidity conditions. (b) Representative cycling stability of the PEDOT:PSS fiber humidity sensor when the RH is cycled 53 % and 31 %.

## References

1. M. Hokazono, H. Anno and N. Toshima, *J. Electron. Mater.*, 2014, **43**, 2196-2201.
2. K. Lim, S. Jung, S. Lee, J. Heo, J. Park, J.-W. Kang, Y.-C. Kang and D.-G. Kim, *Org. Electron.*, 2014, **15**, 1849-1855.
3. J. Nevrela, M. Micjan, M. Novota, S. Kovacova, M. Pavuk, P. Juhasz, J. Kovac, J. Jakabovic and M. Weis, *J. Polym. Sci., Part B: Polym. Phys.*, 2015, **53**, 1139-1146.
4. J. Ouyang, C. W. Chu, F. C. Chen, Q. Xu and Y. Yang, *Adv. Funct. Mater.*, 2005, **15**, 203-208.
5. D. A. Mengistie, P.-C. Wang and C.-W. Chu, *ECS Transactions*, 2013, **58**, 49-56.
6. Z. Yu, Y. Xia, D. Du and J. Ouyang, *ACS Appl. Mater. Interfaces*, 2016, **8**, 11629-11638.
7. Y. Xia, K. Sun and J. Ouyang, *Energ. Environ. Sci.*, 2012, **5**, 5325-5332.
8. J. Ouyang, *ACS Appl. Mater. Interfaces*, 2013, **5**, 13082-13088.
9. Y. Xia, K. Sun and J. Ouyang, *Adv. Mater.*, 2012, **24**, 2436-2440.
10. N. Kim, S. Kee, S. H. Lee, B. H. Lee, Y. H. Kahng, Y.-R. Jo, B.-J. Kim and K. Lee, *Adv. Mater.*, 2014, **26**, 2268-2272.
11. C. Yeon, S. J. Yun, J. Kim and J. W. Lim, *Adv. Electron. Mater.*, 2015, **1**, 1500121.
12. C. M. Palumbiny, C. Heller, C. J. Schaffer, V. Körstgens, G. Santoro, S. V. Roth and P. Müller-Buschbaum, *J. Phys. Chem. C*, 2014, **118**, 13598-13606.
13. H. Okuzaki and M. Ishihara, *Macromol. Rapid Commun.*, 2003, **24**, 261-264.
14. H. Okuzaki, Y. Harashina and H. Yan, *Eur. Polym. J.*, 2009, **45**, 256-261.
15. R. Jalili, J. M. Razal, P. C. Innis and G. G. Wallace, *Adv. Funct. Mater.*, 2011, **21**, 3363-3370.
16. R. Jalili, J. M. Razal and G. G. Wallace, *J. Mater. Chem.*, 2012, **22**, 25174-25182.
17. D. Yuan, B. Li, J. Cheng, Q. Guan, Z. Wang, W. Ni, C. Li, H. Liu and B. Wang, *J. Mater. Chem. A*, 2016, **4**, 11616-11624.
18. J. Zhou, E. Q. Li, R. Li, X. Xu, I. A. Ventura, A. Moussawi, D. H. Anjum, M. N. Hedhili, D.-M. Smilgies, G. Lubineau and S. T. Thoroddsen, *J. Mater. Chem. C*, 2015, **3**, 2528-2538.
19. J. Zhou, M. Mülle, Y. Zhang, X. Xu, E. Q. Li, F. Han, S. T. Thoroddsen and G. Lubineau, *J. Mater. Chem. C*, 2016, **4**, 1238-1249.